Received November 2002
Revised July 2003
Accepted December 2003

Numerical simulations of natural convection around a line-source

Shihe Xin
LIMSI-CNRS, Orsay, France
Dép de Physique, Univ. Paris Sud, Orsay, France
Marie-Christine Duluc, François Lusseyran and Patrick Le Quéré
LIMSI-CNRS, Orsay, France

Keywords *Convection, Boundary layers, Numerical analysis*

Abstract *External natural convection is rarely studied by numerical simulation in the literature due to the fact that flow of interest takes place in an unbounded domain and that if a limited computational domain is used the corresponding outer boundary conditions are unknown. In this study, we propose outer boundary conditions for a limited computational domain and make the corresponding numerical implementation in the scope of a projection method combining spectral methods and domain decomposition techniques. Numerical simulations are performed for both steady natural convection about an isothermal cylinder and transient natural convection around a line-source. An experiment is also realized in water using particle image velocimetry and thermocouples to make a comparison during transients of external natural convection around a platinum wire heated by Joule effect. Good agreement, observed between numerical simulations and experiments, validated the outer boundary conditions proposed and their numerical implementation. It is also shown that, if one tolerates prediction error, numerical results obtained remain at least reasonable in a region near the line-source during the entire transients. We thus paved the way for numerical simulation of external natural convection although further studies remain to be done for higher heating power (higher Rayleigh number).*

Nomenclature

C_p	= specific heat of working fluid at constant pressure (J/kg K)	Pr	= Prandtl number ($=\nu/\kappa$)
$\tilde{C}$	= specific heat of platinum (J/kg K)	q	= heat flux (W/m^2)
D	= cylinder diameter (m)	Q	= heat power or heat loss rate (W)
f	= unknown field	r	= radial distance (m)
g	= gravity acceleration (m/s^2)	R	= cylinder radius (m)
$\mathbf{i}$	= $\sqrt{-1}$	R'	= radial position of the outer boundary (m)
$\bar{I}$	= modified identity matrix	Ra_q	= Rayleigh number based on heat flux ($=[g\beta q R^4]/(\lambda\nu\kappa)$)
k	= azimuthal wave number		
K	= maximum azimuthal wave number	Ra_T	= Rayleigh number based on temperature difference ($=[g\beta\Delta T D^3]/(\nu\kappa)$)
n	= time step		
Nu	= average Nusselt number on the surface of isothermal cylinder	Sf	= r.h.s. term of discrete equation of f
		t	= time (s)

International Journal of Numerical Methods for Heat & Fluid Flow
Vol. 14 No. 7, 2004
pp. 830-850

0961-5539
DOI 10.1108/09615530410546245

Computations have been performed at Centre d'Informatique National de l'Enseignement Supérieur (CINES) under research project lim2072.

T = temperature (K)
u = radial velocity component (m/s)
v = azimuthal velocity component (m/s)
$\vec{V}$ = vector field
p = pressure deviation from hydrostatic pressure (N/m^2)
x = horizontal position (m)
y = vertical position (m)

Greek symbols

β = coefficient of volumetric thermal expansion (K^{-1})
Δ = Laplace operator
ΔT = Superheat on cylinder surface ($T_w - T_0$)
Δt = time step value
ε = small positive value
κ = thermal diffusivity of working fluid (m^2/s)
λ = thermal conductivity of working fluid (W/m K)
$\tilde{\lambda}$ = thermal conductivity of platinum (W/m K)
$\bar{\lambda}$ = $3/(2\Delta t)$
ν = kinematic viscosity of working fluid (m^2/s)
ρ = density of working fluid (kg/m^3)
$\tilde{\rho}$ = density of platinum (kg/m^3)
θ = azimuthal position in polar system
$\Theta = T - T_0$ = superheat (K)

Subscripts and superscripts

k = wave number in Fourier space
n = time step
w = cylinder wall
v = volumetric (per volume)
0 = related to initial or ambient condition
$*$ = predicted velocity field

1. Introduction

Although external natural convection has been studied in the past (similarity solutions, experiments, etc.) (Fuji *et al.*, 1973; Ostroumov, 1956; Schorr and Gebhart, 1970; Yosinobu *et al.*, 1979), it is still an unexplored domain for numerical simulation, as there have been few numerical investigations of such flows (Farouk and Güçeri, 1981; Kelkar and Choudhury, 2000; Kuehn and Goldstein, 1980; Linan and Kurdyomov, 1998; Saitoh *et al.*, 1993; Wang *et al.*, 1990).

External natural convection takes place in an infinite fluid medium or in a fluid medium whose size is large compared with that of the heating element. When trying to study external natural convection by numerical simulation, sometimes one can use a very large computational domain but most of the time one has to limit the computational domain to a small fluid region surrounding the heating element because considering the whole fluid medium is either impossible or too expensive. In the pioneering works (Farouk and Güçeri, 1981; Kuehn and Goldstein, 1980), external natural convection around a horizontal cylinder is studied numerically; the Navier-Stokes equations in stream function-vorticity formulation are solved by using finite differences method and inflow and outflow boundary conditions at an artificially placed outer boundary. For an isothermal cylinder, only local Nusselt number along cylinder surface and averaged Nusselt number are compared with experimental measurements and used to assess the validity of numerical results. Later, Wang *et al.* (1990) revisited the same problem with the same inflow and outflow boundary conditions and pointed out that these outer boundary conditions may be only valid in the steady conditions. As indicated in Saitoh *et al.* (1993), the outer boundary conditions used in Wang *et al.* (1990) do not give the correct results including streamlines and Nusselt number around the cylinder and there is no benchmark solution for this standard problem. This led Saitoh *et al.* (1993) to propose benchmark

solutions to natural convection around a horizontal circular cylinder by using higher accuracy methods (fourth-order finite differences) and a solid boundary condition placed at some 1,000-20,000 times the cylinder diameter. Recently, Linan and Kurdyomov (1998) analytically and numerically investigated natural convection around a line heat source at small Grashof numbers. Solutions at far-field are known analytically; numerical solutions close to the line source are obtained by using finite differences and far-field analytical solutions as inflow boundary conditions and they are used to determine constants involved in analytical expressions of the near-field solutions. Note that these numerical simulations of external natural convection (Farouk and Güçeri, 1981; Kuehn and Goldstein, 1980; Linan and Kurdyomov, 1998; Saitoh *et al.*, 1993; Wang *et al.*, 1990) have been entirely performed in stream function-vorticity formulation.

Although using a very large computational domain can provide benchmark solutions to external natural convection around a horizontal cylinder, obtaining correct streamlines and reasonable results with a relatively small computational domain and artificial outer boundary conditions still makes sense and is challenging, especially for transient external natural convection.

Using a limited fluid region surrounding the heating element as the computational domain gives rise to two questions. Where should we put the external boundary of the limited computational domain? Which kind of boundary conditions must we use on the external boundary that is both inflow and outflow? In order to answer these questions, we proposed artificial conditions at the outer boundary of the limited computational domain and developed a 2D spectral (Chebyshev collocation and Fourier Galerkin) time stepping (projection) code associated with a domain decomposition technique to perform numerical simulations of external natural convection around both an isothermal cylinder and a line-source. The Navier-Stokes equations under velocity-pressure formulation in polar coordinates are discretized in time by a second-order scheme of finite differences type and in space by Fourier Galerkin method in the azimuthal direction. In the radial direction, the circular computational domain is divided into several sub-domains of different sizes so that away from the line-source grids become coarser and in each sub-domain we use Chebyshev collocation method for spatial discretisation. On the interfaces between sub-domains, a C^1 condition is used, i.e. functions and their first normal derivatives are imposed to be continuous. The velocity-pressure coupling is handled by projection method.

Apart from our earlier study (Duluc *et al.*, 2003) only one work has been realized under velocity-pressure formulation (Kelkar and Choudhury, 2000). Furthermore, most of the earlier studies are only devoted to steady external natural convection. This is why the present study is performed under velocity-pressure formulation and particular attention has been paid to transient external natural convection. In Duluc *et al.* (2003), we showed that, for the benchmark problem of natural convection around a horizontal isothermal cylinder, different outer boundary conditions yielded the same Nusselt number, but different flow structures. Steady temperature field near the cylinder is to some extent insensitive to computational domain size, numerical methods and outer boundary conditions. We also showed scalings with heating power in transient external natural convection about a line-source. Owing to the lack of experimental results, no conclusion was drawn on the flow structure in Duluc *et al.* (2003). This is why we set up an experiment and measured velocity field by particle image

velocimetry (PIV) in order to validate the numerical methods used and show the feasibility of numerical simulation of external natural convection. The present work focuses on the numerical methods used, numerical implementation of the outer boundary conditions proposed, flow structure of external natural convection and influence of computational size on flow structure. It concerns mainly transient external natural convection around a line-source, and deals also with steady natural convection about a horizontal isothermal cylinder.

The present paper is organized as follows. In the next two sections we will detail the governing equations of the physical problem studied and the numerical methods proposed. We will then give a brief description of the experiments performed for validating the numerical methods used. Numerical results and comparison between numerical simulations and experiments will be discussed before drawing the final conclusions.

2. Physical problem and governing equations

We are interested in fluid motion around a horizontal heating cylinder of radius R (Figure 1). The cylinder could be either isothermal at a constant temperature or a thin metal wire heated at a constant power by Joule effect. At the starting time the wire is submitted to a step of electrical current; the fluid around the wire is heated and moves up. The working fluid (water in experiment) is considered as a Newtonian fluid of density ρ, volumetric expansion coefficient β, thermal diffusivity κ (thermal conductivity λ and specific heat C_p) and kinematic viscosity ν. We assume that fluid

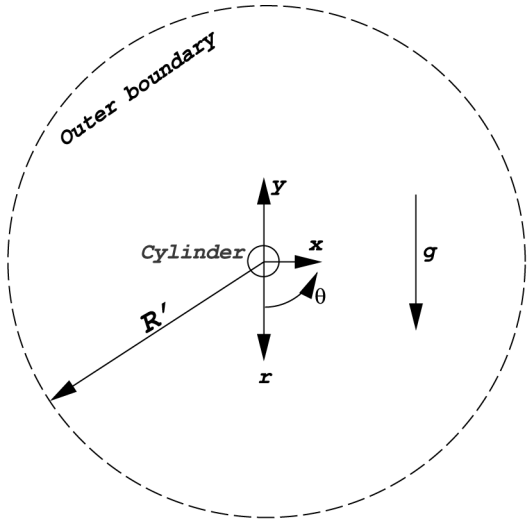

Note: The cylinder could be either isothermal or heated at constant power: in the case of an isothermal cylinder permanent natural convection is studied numerically; in the case of heating at constant power a platinum wire of 50 μm in radius is immersed in distilled water at 293 K and heated by Joule effect and transient natural convection around the wire is studied by numerical simulations and experimental measurements

Figure 1.
External natural convection around a horizontal cylinder

motion is two-dimensional and governed by the following Boussinesq equations (Boussinesq assumption is valid) in polar coordinates:

$$\begin{gathered}\frac{\partial u}{\partial r}+\frac{u}{r}+\frac{1}{r}\frac{\partial v}{\partial \theta}=0\\ \frac{\partial u}{\partial t}+u\frac{\partial u}{\partial r}+\frac{v}{r}\frac{\partial u}{\partial \theta}-\frac{v^2}{r}=-\frac{1}{\rho}\frac{\partial p}{\partial r}+\nu\left[\left(\Delta-\frac{1}{r^2}\right)u-\frac{2}{r^2}\frac{\partial v}{\partial \theta}\right]-g\beta(T-T_0)\cos\theta\\ \frac{\partial v}{\partial t}+u\frac{\partial v}{\partial r}+\frac{v}{r}\frac{\partial v}{\partial \theta}+\frac{uv}{r}=-\frac{1}{\rho r}\frac{\partial p}{\partial \theta}+\nu\left[\left(\Delta-\frac{1}{r^2}\right)v+\frac{2}{r^2}\frac{\partial u}{\partial \theta}\right]+g\beta(T-T_0)\sin\theta\\ \frac{\partial T}{\partial t}+u\frac{\partial T}{\partial r}+\frac{v}{r}\frac{\partial T}{\partial \theta}=\kappa\Delta T\end{gathered} \tag{1}$$

where

$$\Delta=\frac{\partial^2}{\partial r^2}+\frac{1}{r}\frac{\partial}{\partial r}+\frac{1}{r^2}\frac{\partial^2}{\partial \theta^2},$$

t is the time, u and v are the radial and azimuthal velocity components, p is the pressure deviation from the hydrostatic pressure and T is the temperature.

In the case of an isothermal horizontal cylinder, the computational domain, $(r,\ \theta)\in[R,\ R']\times[0,\ 2\pi]$ and the boundary conditions on the cylinder surface $(r=R)$ are

$$\begin{cases}u=v=0\\ T=T_w\end{cases} \tag{2}$$

In the case of a platinum wire heated by Joule effect, in order to consider the wire thermal inertia, equation (1) should be coupled with the heat conduction equation

$$\tilde{\rho}\tilde{C}\frac{\partial T}{\partial t}=\tilde{\lambda}\Delta T+Q_v \tag{3}$$

where Q_v, a uniform volumetric heat source, represents heat power supplied by Joule effect. Then the computational domains for temperature and velocity are $(r,\theta)\in[0,\ R']\times[0,2\pi]$ and $(r,\theta)\in[R,R']\times[0,2\pi]$. Initial conditions for the problem described by equations (1) and (3) are $u=v=0$ and $T=T_0$. Boundary conditions on the wire surface $(r=R)$ are

$$\begin{cases}u=v=0\\ \lambda\left.\dfrac{\partial T}{\partial r}\right|_{\text{fluid}}=\tilde{\lambda}\left.\dfrac{\partial T}{\partial r}\right|_{\text{wire}}\end{cases} \tag{4}$$

At the outer boundary $(r=R')$ the conditions are unknown and we propose the following conditions:

$$\begin{cases} \nu\left(\dfrac{\partial}{\partial r}+\dfrac{1}{r}\right)u=\dfrac{p}{\rho} \\ \nu\left(\dfrac{\partial}{\partial r}+\dfrac{1}{r}\right)v=0 \end{cases} \tag{5}$$

and

$$\left.\frac{\partial T}{\partial r}\right|_{R'}=\left.\frac{\partial T}{\partial r}\right|_{R'-\varepsilon} \tag{6}$$

where ε, a small positive real value, will be taken as the mesh size at $r = R'$.

Note that equation (5) is derived by assuming the balance between pressure and friction in equation (1) and degenerating them in the radial direction (Guermond and Quartapelle, 1998). Equation (6) means that radial derivative of temperature at the outer boundary is equal to that at the first inner point. When compared with the artificial conditions used earlier at the outer boundary (Farouk and Güçeri, 1981; Kelkar and Choudhury, 2000; Kuehn and Goldstein, 1980; Linan and Kurdyomov, 1998; Saitoh *et al.*, 1993; Wang *et al.*, 1990), equations (5) and (6) are linked neither to the inflow nor to outflow at the outer artificially placed boundary. As they do not need only *a priori* knowledge of inflow and outflow at the outer boundary, they need only to be implemented once in a code without extra tests and seem to be more convenient to transient external natural convection if they are validated.

3. Numerical methods

3.1 Time discretization

Equations (1) and (3) are discretized by a second-order time stepping of finite difference type: nonlinear terms are treated explicitly and diffusion is treated implicitly. When applied to an advection-diffusion equation

$$\frac{\partial f}{\partial t}+\vec{V}\cdot\nabla f=\nabla^2 f$$

the time scheme reads

$$\frac{3f^{n+1}-4f^{n}+f^{n-1}}{2\Delta t}+2\vec{V}\cdot\nabla f^{n}-\vec{V}\cdot\nabla f^{n-1}=\nabla^2 f^{n+1}$$

where Δt is the time step. This equation can be cast in a Helmholtz equation for the unknown field f at time $n + 1$:

$$\nabla^2 f^{n+1}-\bar{\lambda}f^{n+1}=Sf$$

where $\bar{\lambda}=3/2\Delta t$. By noting $\Theta = T - T_0$, equations (1) and (3) are discretized in time then read for $r < R$:

$$\left(\tilde{\lambda}\Delta-\frac{3\tilde{\rho}\tilde{C}}{2\Delta t}\right)\Theta^{n+1}=S\Theta \tag{7}$$

and for $R < r < R'$:

$$\begin{cases} \left[\kappa\Delta - \dfrac{3}{2\Delta t}\right]\Theta^{n+1} = S\Theta, \\ \dfrac{\partial u^{n+1}}{\partial r} + \dfrac{u^{n+1}}{r} + \dfrac{1}{r}\dfrac{\partial v^{n+1}}{\partial \theta} = 0, \\ \nu\left[\left(\Delta - \dfrac{1}{r^2}\right)u^{n+1} - \dfrac{2}{r^2}\dfrac{\partial v^{n+1}}{\partial \theta}\right] - \dfrac{3}{2\Delta t}u^{n+1} = \dfrac{1}{\rho}\dfrac{\partial p^{n+1}}{\partial r} + Su + g\beta\Theta^{n+1}\cos\theta, \\ \nu\left[\left(\Delta - \dfrac{1}{r^2}\right)v^{n+1} + \dfrac{2}{r^2}\dfrac{\partial u^{n+1}}{\partial \theta}\right] - \dfrac{3}{2\Delta t}v^{n+1} = \dfrac{1}{\rho r}\dfrac{\partial p^{n+1}}{\partial \theta} + Sv - g\beta\Theta^{n+1}\sin\theta \end{cases} \tag{8}$$

3.2 Spatial discretization

Spectral methods, known to be of infinite order provided that solutions to be approached are regular, are used for spatial discretization. The periodicity in the azimuthal direction naturally leads us to a spatial approximation based on the Fourier series:

$$f(r, \theta) = \sum_{k=-K}^{K} f_k(r)\exp(\mathbf{i}k\theta)$$

Equations (7) and (8) are reduced to the following $(2K + 1)$ 1D problems in r:

$$\left[\tilde{\lambda}\left(\frac{\partial^2}{\partial r^2} + \frac{1}{r}\frac{\partial}{\partial r} - \frac{k^2}{r^2}\right) - \frac{3\tilde{\rho}\tilde{C}}{2\Delta t}\right]\Theta_k^{n+1} = S\Theta_k \tag{9}$$

for $r < R$ and $R < r < R'$

$$\begin{cases} \left[\kappa\left(\dfrac{\partial^2}{\partial r^2} + \dfrac{1}{r}\dfrac{\partial}{\partial r} - \dfrac{k^2}{r^2}\right) - \dfrac{3}{2\Delta t}\right]\Theta_k^{n+1} = S\Theta_k \\ \dfrac{\partial u_k^{n+1}}{\partial r} + \dfrac{u_k^{n+1}}{r} + \dfrac{\mathbf{i}k}{r}v_k^{n+1} = 0, \\ \nu\left[\left(\dfrac{\partial^2}{\partial r^2} + \dfrac{1}{r}\dfrac{\partial}{\partial r} - \dfrac{k^2+1}{r^2}\right)u_k^{n+1} - \dfrac{2\mathbf{i}k}{r^2}v_k^{n+1}\right] - \dfrac{3u_k^{n+1}}{2\Delta t} = \dfrac{1}{\rho}\dfrac{\partial p_k^{n+1}}{\partial r} + Su_k + g\beta\dfrac{\Theta_{k-1}^{n+1} + \Theta_{k+1}^{n+1}}{2}, \\ \nu\left[\left(\dfrac{\partial^2}{\partial r^2} + \dfrac{1}{r}\dfrac{\partial}{\partial r} - \dfrac{k^2+1}{r^2}\right)v_k^{n+1} + \dfrac{2\mathbf{i}k}{r^2}u_k^{n+1}\right] - \dfrac{3v_k^{n+1}}{2\Delta t} = \dfrac{\mathbf{i}k}{\rho r}p_k^{n+1} + Sv_k - g\beta\dfrac{\Theta_{k-1}^{n+1} - \Theta_{k+1}^{n+1}}{2} \end{cases} \tag{10}$$

It is interesting to note that in equation (10) Helmholtz equations of u_k^{n+1} and v_k^{n+1} are coupled. The coupling is alleviated by the change of variables $u_k^+ = u_k + \mathbf{i}v_k$ and $u_k^- = u_k - \mathbf{i}v_k$. Furthermore, $k = 0$, divergence free and boundary conditions lead to $u_0 = 0$ and the momentum equation for u_0 turns out to be the equation for p_0.

In order to get stretched meshes the computational domain in r is divided into sub-domains of different sizes. Figure 2 shows a typical grid used in the case of an isothermal horizontal cylinder. Equations (9) and (10) are then discretized in each sub-domain by using Chebyshev collocation method (Canuto *et al.*, 1988) and are coupled through conditions on the interfaces between the sub-domains. In the radial direction, in each fluid sub-domain the variables are defined at grid points which are a mapping of the Gauss-Lobatto points $[-1, 1]$ (Canuto *et al.*, 1988) and the platinum wire temperature is defined on the Gauss-Radau points (Canuto *et al.*, 1988). In each sub-domain, discrete operators of the first and second derivatives in r are constructed classically by differencing the corresponding polynomials of Lagrange interpolation on the grid points and they are full matrices.

As equations (9) and (10) consist of 1D Helmholtz equations (second-order) for u_k, v_k and Θ_k, the natural conditions on the sub-domain interfaces are that these functions are C^1, i.e. their values and first normal derivatives are continuous. It is known that the global discrete problem in matrix form has block-structure and that the coupling between blocks comes from the conditions on the interfaces (Karageorghis and Paprzycki, 1999). One may solve the global problem by a direct method, but it is more interesting to exploit the block-structure of the global matrix: first solve the Schur complement problem governing the unknown on the interfaces and then the independent block-by-block problems (Smith *et al.*, 1996). In Funaro *et al.* (1988), Louchart *et al.* (1998) and Zanolli (1987), the Schur complement problem (continuity of the function and its first normal derivative) is solved by iterative methods. In the

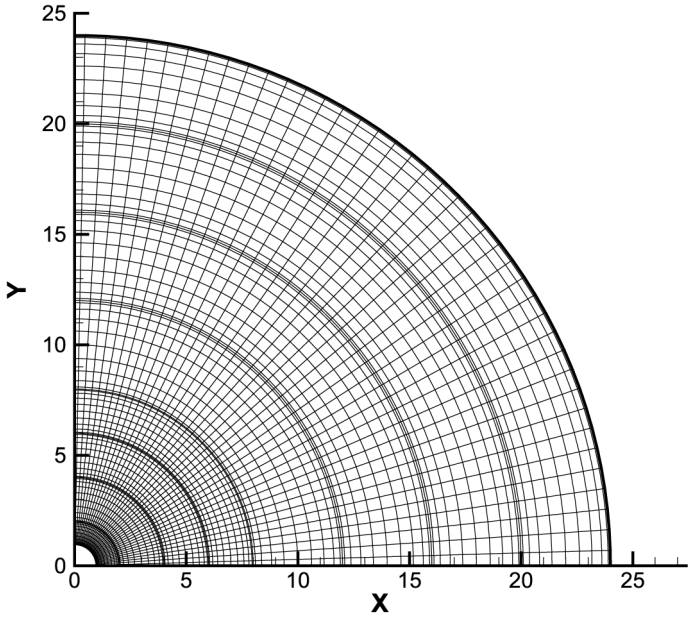

Note: There are 8 sub-domains: one of size R, three of $2R$ and four of $4R$ and only every other points are shown

Figure 2.
Typical grid used in domain decomposition around a horizontal cylinder

present work, we used influence matrix technique or capacitance technique and a 2-iteration method to solve Schur complement problem in order to guarantee the interface conditions: the idea is to impose Dirichlet conditions on the interfaces and release the constraint on the first normal derivative; as there is a linear relationship between the function values on the interfaces and the jump of its first normal derivative through the interfaces, i.e. the Schur complement, in a pre-processing step influences matrix (capacitance) technique that is used to construct this linear relationship by using a complete set of canonical unit vectors of function values on the interfaces and the Schur complement is then a inversed direct method. The solution of the global problem can then be obtained as follows. In the first iteration, a test Dirichlet condition is given on the interfaces and the independent block problems are solved; in the second iteration, the jump of the first normal derivative on the interfaces is calculated, the correction to test the Dirichlet condition is recovered by doing matrix-vector product between the inversed Schur complement and the derivative jump on the interfaces and the right solution of the global problem is finally obtained by solving the independent block problems with the corrected Dirichlet condition on the interfaces.

Note that in the case of a platinum wire equations (9) and (10) are coupled through the temperature condition at $r = R$ which implies energy conservation and takes the following form:

$$\lambda \left.\frac{\partial \Theta_k}{\partial r}\right|_{\text{fluid}} = \tilde{\lambda} \left.\frac{\partial \Theta_k}{\partial r}\right|_{\text{wire}} \tag{11}$$

This condition couples the solid platinum domain with the first fluid sub-domain and can also be considered as an interface coupling between the sub-domains. It is, therefore, part of the Schur complement of the global temperature problem.

3.3 Velocity-pressure coupling

Divergence free flow field can be obtained either by Uzawa methods (Bernard and Maday, 1992; Canuto *et al.*, 1988) or by projection method. We will detail in the following the implementation of the condition (5) in the scope of a projection method consisting of two steps.

In the first step (prediction), we solve the momentum and energy equations (9) and (10) by dropping the divergence-free condition and using the pressure field p^n instead of p_k^{n+1}. We then obtain Θ_k^{n+1} and a predicted velocity field $\left(u_k^*, v_k^*\right)$ which is not divergence free. The corresponding outer boundary conditions to be used are:

$$\begin{cases} \left.\dfrac{\partial \Theta_k^{n+1}}{\partial r}\right|_{R'} = \left.\dfrac{\partial \Theta_k^{n+1}}{\partial r}\right|_{R'-\varepsilon} \\ \nu\left(\dfrac{\partial}{\partial r} + \dfrac{1}{r}\right) u_k^* = 2\dfrac{p_k^n}{\rho} - \dfrac{p_k^{n-1}}{\rho} \\ \nu\left(\dfrac{\partial}{\partial r} + \dfrac{1}{r}\right) v_k^* = 0 \end{cases} \tag{12}$$

Note that the pressure field is extrapolated at the time step $n + 1$.

The second step consists of projecting $\left(u_k^*, v_k^*\right)$ on the divergence free sub-space and we therefore, solve for $k \neq 0$

$$\left[\left(\frac{\partial}{\partial r}+\frac{1}{r}\right)\bar{I}\frac{\partial}{\partial r}-\frac{k^2}{r^2}\right]\frac{p_k^{n+1}-p_k^n}{\rho}=-\frac{3}{2\Delta t}\left(\frac{\partial u_k^*}{\partial r}+\frac{u_k^*}{r}+\frac{\mathbf{i}k}{r}v_k^*\right) \tag{13}$$

where $\bar{I}$ is a modified identity matrix whose first element is equal to zero in order to consider the fact that on the wire surface $u_k^*=0$. On the outer boundary ($r=R'$) we impose:

$$\frac{p_k^{n+1}-p_k^n}{\rho}=-\frac{\mathbf{i}k}{r}v_k^*-\frac{p_k^n}{\rho} \tag{14}$$

which is obtained from equation (5) and the continuity equation.

Equation (13) is discretized in each sub-domain and, apart from the sub-domain adjacent to the wire surface, equations to be solved are Poisson equations. Dirichlet conditions are imposed on the sub-domain interfaces and the Schur complement is used, in the same way as for velocity and temperature, to recover the continuity of the first normal derivative of the pressure correction on the interfaces.

4. Experimental set-up

As mentioned in the "Introduction" there are few numerical simulations of external natural convection due to unknown external boundary conditions and no experimental measurements of velocity field available. The validation of the numerical methods and the external boundary conditions proposed suffers from the lack of results to be compared with. This is why we conducted our own experiments. A line heat source is realized using a thin wire immersed in a liquid filled container and at $t=0$ an electrical current step is used to heat the wire by Joule effect.

In an early study (Duluc *et al.*, 2003), a bronze wire of 20 μm radius and 5.1 cm length has been used and the working fluid was saturated with liquid nitrogen. Since bronze is thermoresistive, the wire is both a heater and a thermometer. Wire temperature measured through its electrical resistance has been compared with the numerical results. Even though the end effects are observed, they are limited to 20 percent of total length near the wire edges. It has been shown that at steady-state, 2D numerical simulations agree well with the measured temperature at the central section. Owing to the end effects, however, numerical results of transient natural convection had not been fully validated.

In order to make a full validation of the present numerical methods, we set-up a new experiment. A platinum wire of 50 μm radius and 5 cm length is immersed in a rectangular cavity made of plexiglass and filled with distilled water, the cavity dimensions are of 50 cm $\times$ 7 cm $\times$ 20 cm (length $\times$ width $\times$ height). Experiments are conducted at room temperature; both temperature in water and velocity field are measured. Temperature measurements are performed using a *K*-type thermocouple of 12.7 μm diameter and PIV techniques are used to measure the velocity field. In the PIV set-up, a vertical laser light sheet perpendicular to the horizontal wire, silver coated hollow spheres of borosilicate glass with smooth surface (diameter of 10 μm and density 1.4) as seeds and a CCD camera of 8 bits (768 $\times$ 484 pixels) are used. Each recording of transients consists of a series of 600 pictures with a time delay of 1/15 s between frames and corresponds to 40 s of observation time. Instantaneous 2D velocity field is obtained from a pair of frames by an original method which is based on optical

flow algorithm rather than on classical cross-correlation. This method allows a finer spatial resolution of the velocity field and is more robust against noise.

More details about the experimental set-up and methods can be found in Duluc *et al.* (2003) and Quénot *et al.* (1998).

5. Results and discussions

In this section, we will focus on two cases: permanent natural convection around a horizontal isothermal cylinder and the experimental case corresponding to transient natural convection around a line-source. The former is used to assess the numerical methods and the proposed outer boundary conditions by comparison with other numerical results (Saitoh *et al.*, 1993 among others) and the latter is used to validate our numerical methods and outer boundary conditions through experiment.

5.1 Isothermal cylinder: a benchmark problem

For natural convection around an isothermal horizontal cylinder, earlier studies used Rayleigh number based on cylinder diameter and temperature difference, Ra_D. In the present study, the case with $\mathrm{Ra}_D = 10^4$ and $\mathrm{Pr} = 0.7$ is investigated in order to show that the proposed outer boundary conditions work also at high Rayleigh number regime. Apart from the average Nusselt number on the cylinder surface only qualitative results on flow structure are presented.

Numerical simulations have been performed with $R' = 24R$ and in total, eight fluid sub-domains as shown in Figure 2 have been used. In the azimuthal direction, we used $K = 120$ and in each sub-domain 21 Gauss-Lobatto points have been used to discretize equation (10) in the radial direction.

Starting from motionless flow condition and after the transient, time evolution of Nu indicates that a quasi-permanent regime is reached normally and that the proposed outer boundary conditions do not seem to cause any difficulty for numerical procedure to converge. Flow structure corresponding to the quasi-steady-state indicated by Nu is shown in Figure 3. One distinguishes the lower part of thermal plume and outside the thermal plume the incoming flow is downwards, which is somewhat strange and is not consistent with the flow structure given in Saitoh *et al.* (1993) by using a very large computational domain. However, the value of Nu is equal to 4.791, which agrees well with 4.826 in Saitoh *et al.* (1993). We kept integrating the quasi-permanent solution and obtained steady-state solution which is also shown in Figure 3. Outside the thermal plume the incoming flow is more horizontal but always downwards. Although flow structure evolved slightly, Nu which decreased only to 4.784 remained almost constant. This suggests that temperature field is insensitive to flow structure outside the thermal plume and that using only Nusselt number is not enough to validate flow structure outside the thermal plume.

In order to assess the validity of the predicted flow structure, i.e. to know where the predicted flow is reasonable and where it is not, more detailed results of velocity fields are needed; for example, velocity profiles at fixed x and y positions.

5.2 Transient natural convection around a line-source

In the experiment, a line-source is represented by a platinum wire of 50 μm radius heated by Joule effect. The heating power is $Q_v = 3.8 \times 10^9\ \mathrm{W/m^3}$ (which is equivalent to a surface heat flux of $q = 9.5 \times 10^4\ \mathrm{W/m^2}$) and the room temperature, T_0, is equal to

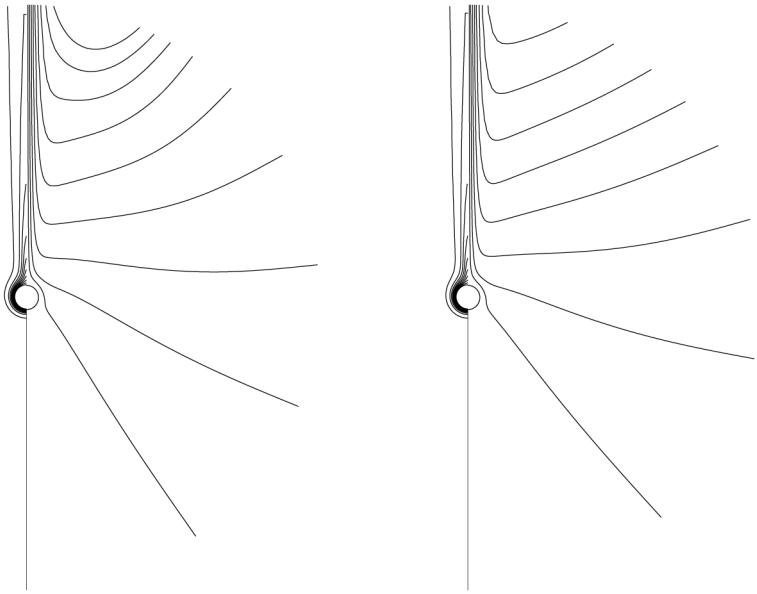

Figure 3.
Flow structure (temperature and stream function) around an isothermal cylinder (quasi-steady-state, left; permanent regime, right) $\mathrm{Ra}_D = 10^4$ and $\mathrm{Pr} = 0.7$

293 K. If we define a Rayleigh number based on heat flux, $\mathrm{Ra}_q = g\beta qR^4/\lambda\nu\kappa$ is very small value, approximately equal to 0.015.

5.2.1 Comparison between numerical and experimental results. In this subsection, we will compare in detail the experimental measurements with numerical results to validate the external boundary conditions (5) and (6) and their numerical implementations. Numerical simulations have been performed in a computational domain with $R' = 3.025\,\mathrm{cm}$ ($\approx 600\,R$).

As soon as the wire is heated up, water around it is also warmed up through heat conduction. As warm water tends to move upwards, convective motion sets up and squeezes circular isotherms and a thermal plume, in the form of a mushroom, for the temperature field observed. The "mushroom" is growing in time as shown in Figure 4.

The "mushroom" structure of temperature field is induced by the onset of convection, especially by the set-up of two initial vortices (Figure 4). We can compare the positions of vortex center, which is below the round top of the mushroom, calculated from numerical simulations and measured in experiments. The results obtained are shown in Figure 5, they show a good agreement between the numerical simulations and experiments. Both results indicate that the vortex centers evolve in time by following straight lines and the numerical simulations performed seem to predict reasonably the transient behavior of the thermal plume. From these straight lines it is easy to determine the virtual source point which is located below the wire and from which initial vortices are generated. This is quite similar to the idea of virtual source for steady thermal plume expansion.

It is to note, however, that in numerical simulations when the vortices approach the external boundary their centers are deviated from the straight lines they followed. This behavior is not physical and is certainly due to the outer boundary conditions.

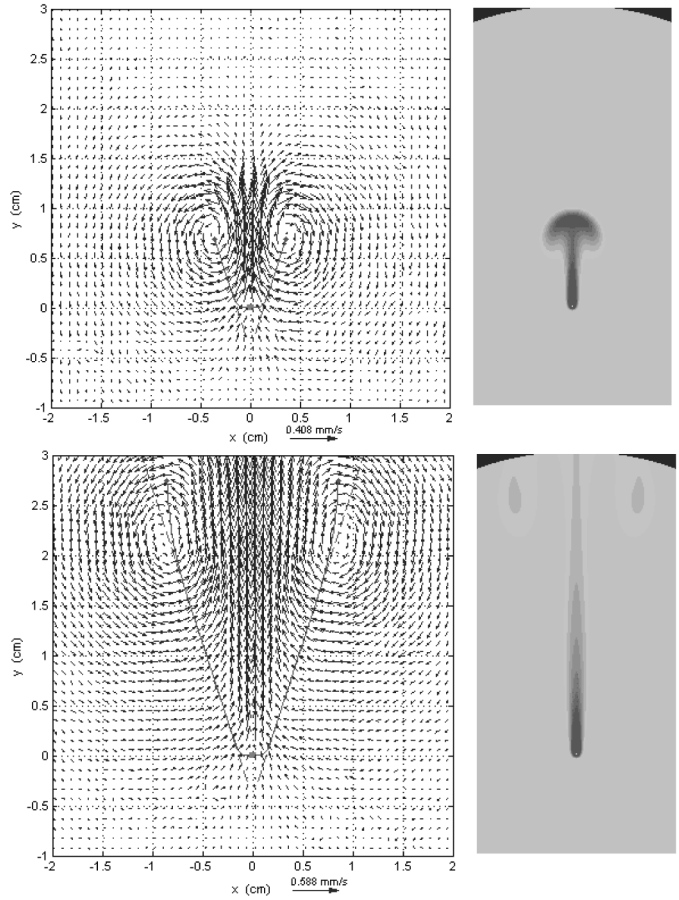

Note: Lines on velocity vectors indicate trajectories of vortex center and the black top part of temperature field shows the boundary of computational domain

Figure 4.
Instantaneous velocity (PIV measurements, left) and temperature (numerical results, right) fields in the same spatial scale at $t = 6$ s (top) and 16 s (bottom)

Therefore, the outer boundary conditions used cannot predict correctly the full transient process, at least not in the entire computational domain. The important question to be answered is whether, in the long-run, the boundary conditions proposed yield reasonable prediction of flow structure. For this purpose, velocity profiles at $t = 16$ s are chosen (i.e. the initial vortices are crossing the outer boundary) and Figure 6 shows the numerical and experimental results at $y = 0.5$ and 2.5 cm (y is the height above the wire). Excellent agreement between the experiment and numerical simulation is observed at $y = 0.5$ cm. Owing to the fact that the trajectories of the initial vortices are artificially modified by the outer boundary conditions, at $y = 2.5$ cm the discrepancy between the results is important for the horizontal velocity component while agreement remains good for the vertical velocity component. Although the outer boundary conditions used influence the trajectories of the initial vortices, long time flow structure of the thermal plume is correctly predicted by the numerical methods

associated with the outer boundary conditions (5) and (6) implemented in the form of equations (12) and (14).

The transient process can be illustrated by time evolution of temperature field. The temperature at $y = 0.67$ cm above the wire is measured experimentally by a thermocouple of 12.7 μm diameter and also calculated numerically (Figure 7). One observes again an excellent agreement between the numerical and experimental results. It takes about 4 s for the mushroom of the thermal plume to grow up to $y = 0.67$ cm, the head of the mushroom which is hotter than the surrounding water passes this position in 2 s (4 s $< t <$ 6 s) and then temperature evolves slowly in time to a constant value.

In comparison with the experimental measurements and with regard to the good agreement observed, we conclude that the outer boundary conditions used are validated. Note, however, that the experimental configuration investigated corresponds to a case of very small Rayleigh number ($\approx$0.015) and that further investigation, both numerical and experimental, is needed to validate the outer boundary conditions (5) and (6) at higher Rayleigh numbers.

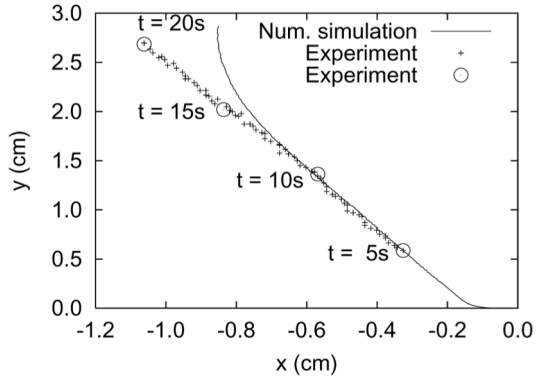

Figure 5.
Measured and computed positions of initial vortex center. Simulations have been conducted with $R' = 3.025$ cm

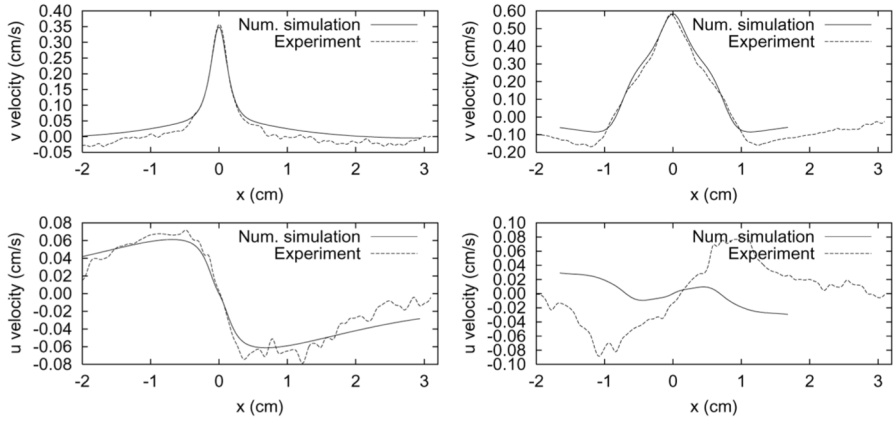

Figure 6.
Velocity profiles (vertical component on top and horizontal at bottom) at $t = 16$ s and $y = 0.5$ (left) and 2.5 cm (right)

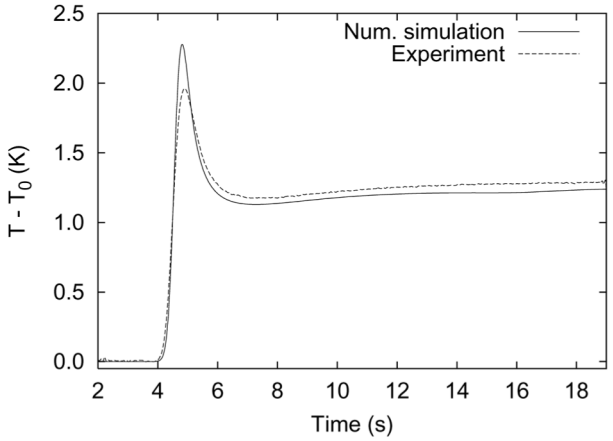

Figure 7.
Time evolution of temperature at $(x, y) = (0, 0.67\,\text{cm})$

Note: Temperature has been measured by a micro-thermocouple of 12.7 μm in diameter

5.2.2 Influence of computational domain size. In order to understand the influence of computational domain size on numerical results when using the external conditions (5) and (6), we performed numerical simulations corresponding to the experimental case with two other computational domains: $R' = 2.065\,\text{cm} = R'_2 (\approx 400\,R)$ and $R' = 1.105\,\text{cm} = R'_3 (\approx 200\,R)$.

Computations realized with $R' = 3.025\,\text{cm} = R'_1$ showed that during the transient the trajectories of the initial vortex centers are deviated from the measured straight lines when the initial vortices approach the external boundary (Figure 5). Computational domain size does not modify this conclusion for the three R' investigated (Figure 8). This means that for a given R' the transient predicted by numerical simulation for the present experimental case, in a region near R' and during

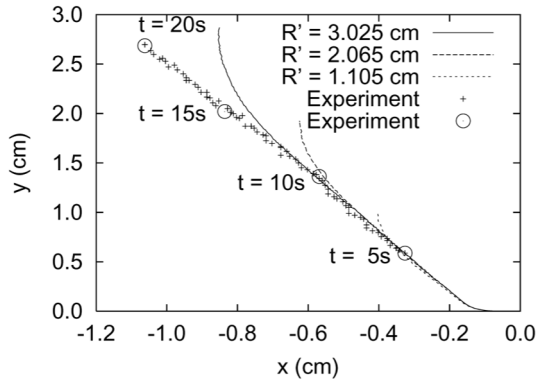

Figure 8.
Influence of computational domain size on positions of initial vortex center

Note: No matter which is the size of computational domain, trajectories of initial vortex center are deviated when the vortices are approaching R'

the period when the initial vortices approach the external boundary, will be different from that really taking place in an unbounded domain.

To better illustrate the effect of the outer boundary conditions, velocity and temperature profiles at $t = 6$ s and at several positions are shown in Figure 9. Time $t = 6$ s is the moment when the "mushroom" top is reaching R'_3 and the initial vortices are crossing this external boundary (Figure 8). The whole set of graphs shown in Figure 9(a) shows that, at this time, results obtained with R'_1 and R'_2 agree well independently of the positions, while numerical simulation performed with R'_3 yields slightly different results. In the last case, the thermal plume in the form of a mushroom grows faster than it should. This is why at $t = 6$ s the position of the mushroom top obtained with R'_3 is above those predicted by the other two simulations (Figure 9(b)). Consequently, at $y = 1$ cm the values of temperature and vertical velocity component calculated with R'_3 are much larger. To some extent the outer boundary conditions (5)

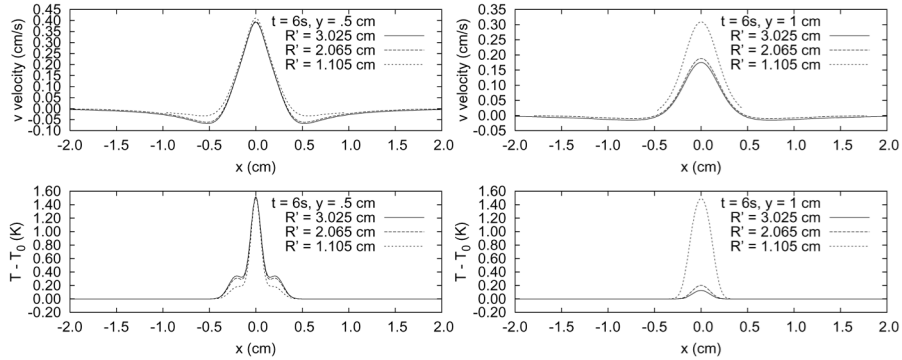

(a) Profiles of vertical velocity and temperature at $y = 0.5$ cm (left) and $y = 1$ cm (right). $t = 6$ s

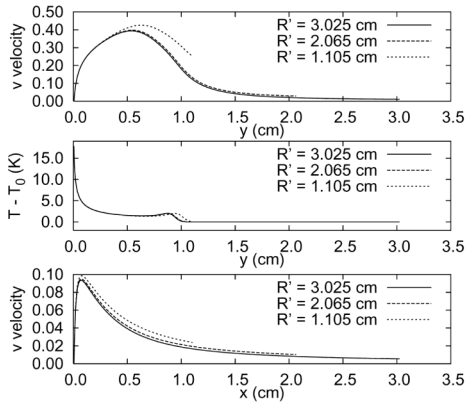

(b) Profiles of vertical velocity (top) and temperature (middle) at $x = 0$ and vertical velocity profile (bottom) at $y = 0$. $t = 6$ s

Figure 9.
Profiles of vertical velocity and temperature at $t = 6$ s

and (6) make the transient process faster in the region near R' during the period when the mushroom head and the initial vortices cross R'. Nevertheless, it is still safe to say that at $t = 6$ s numerical results obtained with R'_3 remain reasonable in the region near the heating wire, i.e. $r < 0.5$ cm ($\approx 100R$), because a good agreement between the numerical results is observed in this region (Figure 9(b)).

Figure 7 also shows that, after the mushroom head travels downstream to a given position, flow field reaches a nearly constant value at this position. It is, thus, interesting to know if the outer boundary conditions influence these constant values or more generally long-time behavior of the flow structure. For this purpose, in Figure 10 we will show different profiles of vertical velocity and temperature obtained at $t =$ 20 s. The surprising fact is that no matter which R' used there is always in good agreement with the numerical results. Therefore, for the case investigated the long-time behavior of flow field is correctly predicted by numerical simulations even

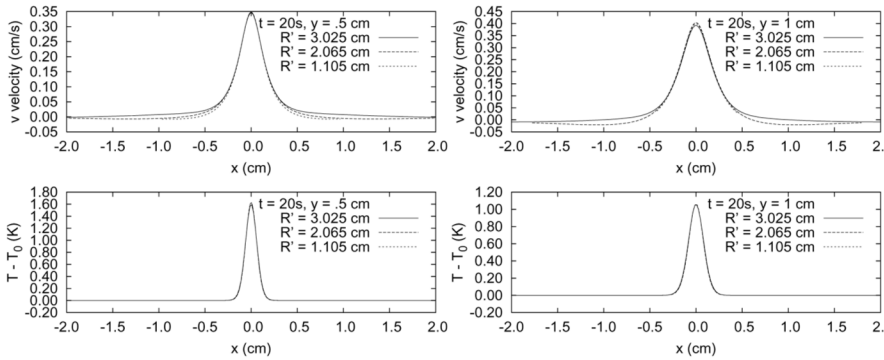

(a) Profiles of vertical velocity and temperature at $y = 0.5$ cm (left) and $y = 1$ cm (right). $t = 20$ s

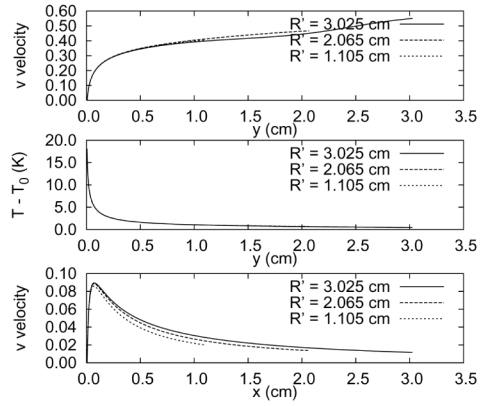

(b) Profiles of vertical velocity (top) and temperature (middle) at $x = 0$ and vertical velocity profile (bottom) at $y = 0$. $t = 20$ s

Figure 10.
Profiles of vertical velocity and temperature at $t = 20$ s

when one uses a computational domain with R'_3 (about 200 times the wire radius). This indicates that the outer boundary conditions (5) and (6) do produce, at least for the experimental case studied, physically meaningful flow structure at long time. Note that long time means long time after the initial vortices exit the computational domain. It depends, therefore, on the size of the computational domain. Long time for smaller computational domains will not be that for larger ones.

As flow conditions at the outer boundary are not disturbed during the initial phase of transients, computational domain can be considered as infinite and the outer boundary conditions should have no influence on the numerical results. This means that no matter which computational domain is used the studied transient can be divided into three phases: an initial phase, a long time phase (permanent regime in the computational domain) and the one in between. For the initial and long time phases the proposed outer boundary conditions predict well the flow structure in the whole computational domain, while during the phase in between numerical solutions are not reasonable everywhere in the computational domain. It is, thus, interesting to quantify the initial phase for a given R' and assess the smallest region insensitive to the outer boundary conditions during the phase in between. Figure 11 shows the end of the initial phase which occurred between 4 and 5 s for R'_3. It is clear that at $t = 5$ s numerical solutions obtained with R'_3 are no more reasonable for $r > 0.4$ cm. In the same way, the end of the initial phase for R'_2 is observed between 7 and 8 s (Figure 12).

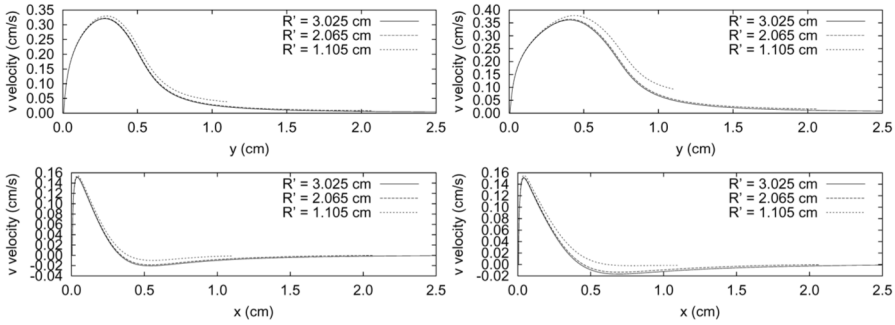

Figure 11.
Profiles of vertical velocity at $x = 0$ (top) and $y = 0$ (bottom); $t = 4$ s (left) and 5 s (right)

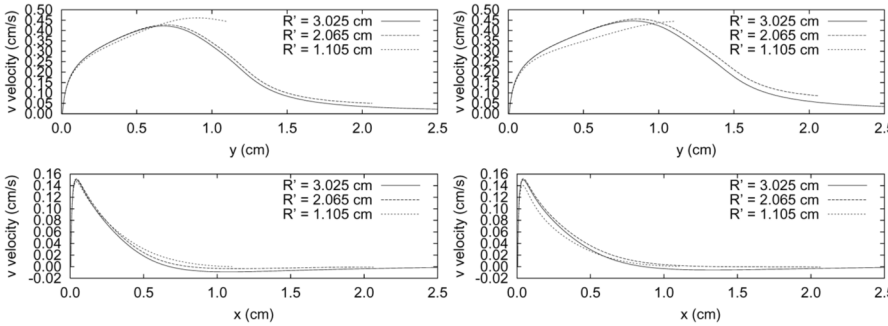

Figure 12.
Profiles of vertical velocity at $x = 0$ (top) and $y = 0$ (bottom); $t = 7$ s (left) and 8 s (right)

Scaling of the positions of maximum vertical velocity at $x = 0$ (above the wire) yielded an empirical law of $0.35R'$ as the end of the initial phase, i.e. as far as the position of the maximum vertical velocity above the wire at $x = 0$ does not exceed $0.35R'$ the numerical solutions are likely to be reasonable everywhere in the computational domain. Figure 12 shows also that during the phase in between the smallest region insensitive to the boundary conditions for R'_3 is inside the position of maximum vertical velocity at $y = 0$ (at the wire level), this also holds for R'_2. Any tolerance of prediction error will enlarge the smallest region insensitive to the boundary conditions.

The three computational domains used possess a common region which is $r \leq R'_3$. It is interesting to use the three sets of solutions obtained in $r \leq R'_3$ in order to obtain extrapolated solutions which would be independent of domain size. Figure 13 shows the extrapolated solutions given by using quadratic extrapolation in the common region at $t = 6$ and 20 s. As for R'_1, $t = 6$ s is in the initial phase and solution obtained with R'_1 is a good prediction of what should happen in an infinite domain, solutions have been extrapolated to $R' = 800\,R$.At$t = 20$ s, quadratic extrapolation has been done to $R' = 1,000\,R$. At $t = 6$ s, thermal plume of mushroom structure is approaching the outer boundary at R'_3 and part of initial vortices is out of the computational domain. It is another form of flow fields shown in Figure 4. At $t = 20$ s inside R'_3, only the lower part of the thermal plume is observed and fluid motion is mainly upwards. This is in qualitative agreement with flow structures shown in Linan and Kurdyomov (1998) for small Grashof numbers.

6. Concluding remarks

In order to pave the way for numerical simulations of external natural convection and the corresponding transients, we implemented, for solving the Navier-Stokes equations under Boussinesq assumption in velocity-pressure formulation, a

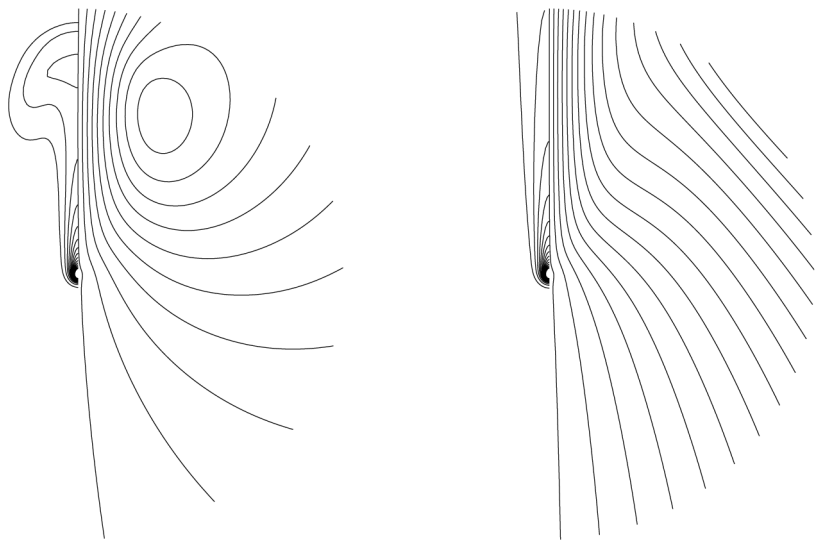

Figure 13.
Extrapolated solutions (temperature and stream function) in R'_3 at $t = 6$ s (left) and 20 s (right) around a line-source

numerical code using spectral methods, domain decomposition technique with Schur complement, projection method (velocity-pressure coupling) and new outer boundary conditions.

The validation of the code implemented was done through performing experimental measurements. A thin platinum wire heated by Joule effect has been used in the experiment to represent a line-source and Rayleigh number investigated, Ra_q, is about 0.015. During the transient, time evolution of pointwise temperature is measured by micro-thermocouples and velocity field by PIV. Numerical results agree well with the experimental data and the code implemented (numerical methods and outer boundary conditions used) was thus validated.

Numerical simulations were also realized for the experimental case in order to reveal the influence of computational domain size on numerical results. It is shown that the proposed boundary conditions (5) and (6) make transient process faster than it should be when the initial vortices approach the external boundary. It is also shown that the numerical results obtained at long time in the experimental case predict well the flow structure in the whole computational domain. No matter which computational domain size R' is, the transient of the experimental case, yielded by numerical simulations using the proposed outer boundary conditions, can be divided into three phases: the initial phase, the long time phase and the one in between. During the initial and long time phases, numerical results are reasonable everywhere in the computational domain. The end of the initial phase is defined by the time when the vertical position of maximal vertical velocity above the wire at $x = 0$ exceeds $0.35R'$ and the long time phase means long time after the initial vortices exit the computational domain. During the phase in between, the present numerical results are not reasonable everywhere: the smallest region which is insensitive to the outer boundary conditions is inside the position of maximum vertical velocity at $y = 0$. This region can be enlarged provided some tolerance of prediction error. If prediction error can be accepted to some extent, numerical simulation of transient external natural convection using the proposed outer boundary conditions is feasible because numerical results obtained are reasonable at least in a region near the line-source during the entire transient.

It is important to point out that Rayleigh number of the testing case is small, the proposed boundary conditions (5) and (6) are at least appropriate for low Rayleigh number cases. Further studies, both experimental and numerical, should be done to validate these conditions at higher Rayleigh numbers. Nevertheless, in order to show that the proposed outer boundary conditions work also at high Rayleigh number, numerical simulations have been done for an isothermal cylinder at $Ra_D = 10^4$ and $Pr = 0.7$ and the average Nusselt number along the cylinder surface obtained agrees well with the results in the literature.

As the position of the outer boundary is chosen to enable numerical simulation of external natural convection and the flow conditions on such a boundary are unknown, one cannot expect that numerical simulations undertaken in this way predicts well the corresponding flow structure everywhere in the whole computational domain. Numerical prediction has, however, to be reasonable and even good in part of the computational domain near the heating element. This is observed from the numerical simulations we performed and should be the rule of validating numerical simulations of external natural convection.

References

Bernard, C. and Maday, Y. (1992), "Approximations spectrales de problèmes aux limites elliptiques", *Collection Mathématiques & Applications*, Springer Verlag, Berlin.

Canuto, C., Hussaini, M., Quarteroni, A. and Zang, T. (1988), *Spectral Methods in Fluid Dynamics*, Springer Verlag, Berlin.

Duluc, M-C., Xin, S. and Le Quéré, P. (2003), "Transient natural convection and conjugate transients around a line heat source", *Int. J. Heat Mass Trans.*, Vol. 46, pp. 341-54.

Farouk, B. and Güçeri, S. (1981), "Natural convection from a horizontal cylinder – laminar regime", *J. Heat Transfer*, Vol. 103, pp. 522-7.

Fujii, T., Morioka, I. and Uehara, H. (1973), "Buoyant plume above a horizontal line heat source", *Int. J. Heat Mass Trans.*, Vol. 16, pp. 755-68.

Funaro, D., Quarteroni, A. and Zanolli, P. (1988), "An iterative procedure with interface relaxation for domain decomposition methods", *SIAM J. Numer. Anal.*, Vol. 25 No. 6, pp. 1213-36.

Guermond, J-L. and Quartapelle, L. (1998), "On the approximation of the unsteady Navier-Stokes equations by finite element projection methods", *Numer. Math.*, Vol. 80 No. 5, pp. 207-38.

Karageorghis, A. and Paprzycki, M. (1999), "Conditioning of pseudospectral matrices for certain domain decomposition", *J. Sci. Comp.*, Vol. 14 No. 1, pp. 107-19.

Kelkar, K. and Choudhury, D. (2000), "Numerical method for the prediction of incompressible flow and heat transfer in domains with specified pressure boundary conditions", *Numer. Heat Transf.* B, Vol. 38, pp. 15-36.

Kuehn, T. and Goldstein, R. (1980), "Numerical solutions to the Navier-Stokes equations for laminar natural convection about a horizontal isothermal circular cylinder", *Int. J. Heat Mass Trans.*, Vol. 23, pp. 971-9.

Linan, A. and Kurdyomov, V. (1998), "Laminar free convection induced by a line heat source and heat transfer from wires at small Grashof numbers", *J. Fluid Mech.*, Vol. 362, pp. 199-227.

Louchart, O., Randriamampianina, A. and Leonardi, E. (1998), "Spectral domain decomposition technique for the incompressible Navier-Stokes equations", *Numer. Heat Transf.* A, Vol. 34, pp. 495-518.

Ostroumov, G. (1956), "Unsteady heat convection near a horizontal cylinder", *Sov. Phys. Tech. Phys.*, Vol. 1 No. 12, pp. 2627-41.

Quénot, C., Pakleza, J. and Kowalewski, T. (1998), "Particle image velocimetry with optical flow", *Exp. Fluids*, Vol. 25, pp. 177-89.

Saitoh, T., Sajiki, T. and Maruhara, K. (1993), "Benchmark solutions to natural convection heat transfer problem around a horizontal cylinder", *Int. J. Heat Mass Trans.*, Vol. 36, pp. 1251-9.

Schorr, A.W. and Gebhart, B. (1970), "An experimental investigation of natural convection wakes above a line heat source", *Int. J. Heat Mass Trans.*, Vol. 13, pp. 557-71.

Smith, B., Bjorstad, P. and Cropp, W. (1996), *Domain Decomposition: Parallel Multilevel Methods for Elliptic Partial Differential Equations*, Cambridge University Press, New York, NY.

Wang, P., Kahawita, R. and Nguyen, T. (1990), "Numerical computation of the natural convection flow about a horizontal cylinder using splines", *Numer. Heat Transf.* A, Vol. 17, pp. 191-215.

Yosinobu, H., Onishi, Y., Enyo, S. and Wakitani, S. (1979), "Experimental study on instability of a natural convection flow above a horizontal line heat source", *J. Phys. Soc. Jpn*, Vol. 47 No. 1, pp. 161-71.

Zanolli, P. (1987), "Domain decomposition algorithms for spectral methods", *Calcolo*, Vol. 24, pp. 202-40.